An amorphous monolayer: Infrared spectroscopic and theoretical studies of SO2 on NaCl (100)

Otto Berg, George E. Ewing, Andrew W. Meredith, and Anthony J. Stone

Citation: The Journal of Chemical Physics **104**, 6843 (1996); doi: 10.1063/1.471351
View online: http://dx.doi.org/10.1063/1.471351
View Table of Contents: http://scitation.aip.org/content/aip/journal/jcp/104/17?ver=pdfcov
Published by the AIP Publishing

An amorphous monolayer: Infrared spectroscopic and theoretical studies of SO_2 on NaCl (100)

Otto Berg[a] and George E. Ewing[c]
Department of Chemistry, Indiana University, Bloomington, Indiana 47405

Andrew W. Meredith[b] and Anthony J. Stone[c]
University Chemical Laboratory, Lensfield Road, Cambridge, CB2 1EW, United Kingdom

(Received 11 December 1995; accepted 17 January 1996)

At temperatures between 100 and 110 K, exposing the (100) face of NaCl to unsaturated SO_2 gas yields a stable adlayer. Infrared spectra of adsorbed SO_2 contain complex resonances near the origins of the molecular symmetric and asymmetric stretching vibrations. On photometric grounds the absolute coverage of the surface is found to be one molecule per exposed Na^+Cl^- ion pair. The spectra of this monolayer consist of several sharp lines overlapping one broad feature for each molecular mode. By comparison to vibrational excitons in simpler systems, the coexistence of crystalline and amorphous adlayer structures is strongly indicated. This partial ordering is pressure dependent, and develops spontaneously on a time scale of minutes. The disordered component, in contrast, is never in equilibrium with the gas phase. Computational simulations have detailed the microscopic basis of this behavior. Accurate *ab initio* models of the SO_2 molecule and NaCl(100) surface were used in a Monte Carlo simulation of the experimental conditions. At both half and full coverage, an amorphous two-dimensional condensate developed. This is minimally consistent with the polarized infrared photometry. Seemingly equilibrated Monte Carlo runs retained some memory of the initial molecular configuration, again consistent with hysteresis observed in the spectroscopic experiments. No structural order developed in the simulations, but the energetic state of affairs was clarified: the potential driving adsorption and condensation is deep in comparison to available thermal energy, but relatively insensitive to molecular orientation. © *1996 American Institute of Physics.* [S0021-9606(96)00716-8]

INTRODUCTION

The (100) faces of single crystal NaCl have been favored surfaces for the infrared spectroscopic study of adlayers of a number of small molecules. Well ordered monolayers of CO,[1,2] CO_2,[3,4] and CH_4[5] have been prepared in equilibrium with their gas phases. At low temperature (<77 K) the spectroscopic features are narrower than 1 cm^{-1}, suggesting that both the adlayer and substrate are structurally homogeneous. The polarization dependence of these features is related to molecular orientation in the layer, while their number and infrared activity depends on the layer's symmetry. Such data have led to structural models that agree with other experiments and computational results. Since the van der Waals diameters of these adsorbates (a measure of how closely they pack into a condensed phase) are less than the lattice constant of NaCl, it is perhaps not surprising that they can form commensurate monolayers. C_2H_2 forms a bilayer on NaCl(100), presumably because of its ability to form relatively strong intermolecular bonds.[6] Yet the vibrational features are sharp, again suggesting a homogeneous adlayer whose structure resembles the bulk crystal structure of C_2H_2.[7] So with few exceptions,[8] we expect small molecules to form a well ordered adlayer on single crystal NaCl(100) with one to three molecules per unit mesh. As we shall see, SO_2 does not fall into this pattern.

The properties of SO_2 are well known. The bent molecule, with van der Waals diameter of 403 pm,[9] is within 2% of the separation of 397 pm for neighboring Na^+ (or Cl^-) ions in the (100) face.[10] Perhaps more to the point, the dimensions of the orthorhombic unit cell of bulk crystalline SO_2 of $a=607$ pm, $b=594$ pm, $c=614$ pm[11] are within 10% of the lattice constant NaCl of $a=562$ pm.[10] [The somewhat less compatible $a=619$ pm, $b=600$ pm, $c=600$ pm unit cell dimensions of bulk crystalline C_2H_2[7] do not prevent this molecule from forming a well ordered adlayer on NaCl(100).[6]] The thermodynamic studies of SO_2 reveal a single crystal phase with evidence[12] of some disorder just below its melting point of 197.6 K. This disorder disappears toward lower temperatures, however, and the entropy approaches zero, indicating a perfect crystalline state in accord with the third law of thermodynamics.[12,13] The vibrational spectroscopy of solid SO_2 shows splittings consistent with expected crystal field effects.[14–16]

Polycrystalline NaCl has been used as a substrate for SO_2 adsorption by Ron and Folman.[17] Isotherm measurements show that the isosteric heat of adsorption (-32 ± 4 kJ/mol) is only slightly larger than the heat of vaporization of SO_2 (-24.9 kJ/mol).[12] This indicates that adsorbate–substrate attraction is comparable to lateral adsorbate–adsorbate interactions. The potential energy of adsorption, as

[a]Present address: Department of Chemistry, University of California, Riverside, CA 92521.
[b]Present address: Department of Physical Chemistry, The University of Göteborg, S-412 96 Göteborg, Sweden.
[c]To whom correspondence should be addressed.

modeled by Ron and Folman, showed that the global minimum of a *single* SO_2 molecule against the (100) face has the O atoms bridging adjacent Na^+ ions with the molecular axis of the dipod perpendicular to the surface. Another minimum, also with the molecular axis perpendicular to the surface, has the S atom toward the Cl^- ion. Ron and Folman also documented the dependence of dielectric relaxation rates on temperature in the SO_2/NaCl system. These rates are consistent with thermally activated fluctuations between the two adsorption geometries identified by theory. Nevertheless, there are many indications that lateral interaction among SO_2 molecules influences the formation of these layers. A more realistic computational model is called for.

The intermolecular potential governing SO_2 clusters has been studied by Bone *et al.*[18] They explored stationary points on the $(SO_2)_2$ and $(SO_2)_3$ potentials by a variety of *ab initio* methods. The surfaces have a number of minima (corresponding to different intermolecular geometries), but these are shallow in comparison to the intermolecular binding energy of the clusters. The dissociation energy (D_e) calculated for a bound dimer with C_s symmetry[19] is 14.8 kJ mol^{-1}. When compared to the heat of adsorption observed by Ron and Folman, it is again clear that an intermolecular contribution to the energetics of a close-packed monolayer is significant.

In the following we present infrared spectra of the SO_2/NaCl(100) system under various conditions, but find reason to doubt that thermodynamic equilibrium was attained. Results of a large-scale computational model are also described; no uniquely stable ordered structure is found. By comparing these results we identify physical properties that tend to trap this system in a disordered or partially ordered state.

SPECTROSCOPIC STUDY

Equipment and procedures

The experimental details are given elsewhere.[1,3] Only information relevant to the reported results is presented here.

Two $30\times20\times3$ mm^3 NaCl crystals were cleaved in air along the (100) plane. These slabs were mounted on a copper sample holder so that the normal to each face was at a 60° angle to the interrogating light beam. The sample holder was attached to an open-cycle liquid helium cryostat. A thermistor and resistive heater were used to control temperature, with an estimated accuracy of ±1 K. Temperature was maintained to within 0.2 K. The crystals and sample holder were enclosed in an ultra high vacuum chamber where an ion pump maintained a base pressure in the 10^{-10} mbar range. Between experiments the crystals were stored at 380 K, because all atmospheric gases desorb at this temperature, but evaporation of the NaCl substrate is minimal. The vacuum chamber was fitted with wedged CaF_2 windows to reduce etalon fringes.

Infrared spectra were recorded using a Fourier transform infrared spectrophotometer (Mattson Nova Cygni 120). The light was directed through a wire grid polarizer (Molectron) and collected onto the element of a liquid nitrogen-cooled MCT detector. E_s polarized light has its electric field vector perpendicular to the plane of incidence (i.e., parallel to the substrate), while E_p light is polarized parallel to the plane of incidence and has electric field vector components perpendicular and parallel to the surface. Resolution ranged from 0.1 to 1 cm^{-1}. Values of absorbance, $A=\log_{10}(I_0/I)$, and integrated absorbance, $\tilde{A}=\int_{\text{band}} \log_{10}(I_0/I)d\tilde{\nu}$, were measured for many bands.

Matheson SO_2 (>99.98%) was purified by repeated freeze–pump–thaw cycles followed by passing the gas through a series of U tubes at 175 K. The final product, as the gas or adlayer, was tested by infrared spectroscopy. No absorption features that could not be assigned to SO_2, or incompletely purged atmospheric H_2O or CO_2, were observed. In recording pressures of SO_2 for the uhv experiments, the pressures read on the ion gauge calibrated for N_2, were divided by a factor of 2.1 to correct for ionization cross section.[20]

Results

Four experimental sets were performed to explore different aspects of the adsorption process.

First, a temperature of 106.3 K was chosen at which the presence and quality of signals changed with pressure in a convenient range (near 10^{-8} mbar). Spectra of apparently stable layers were recorded at points of a pressure cycle at 0.5 cm^{-1} resolution with E_p polarization. Having selected a pressure, the crystals were exposed for 45 min or more in an attempt to achieve an equilibrium between SO_2 in the gaseous and adsorbed phases. A spectrum was then recorded at this pressure. A new pressure was chosen and, after another time interval, the spectrum under these conditions was taken. The pressure was adjusted from a beginning value of 0.5×10^{-8} mbar to a maximum of 4×10^{-8} mbar and then back down to 0.5×10^{-8} mbar. Survey scans covering both the symmetric stretch (ν_1, gas phase origin ~1140 cm^{-1}) and asymmetric stretch (ν_3, gas phase origin ~1330 cm^{-1}) in E_p polarization are shown in Fig. 1 (Periodic spikes at ~50 cm^{-1} intervals are instrumental artifacts.) Considerable variations in spectral profiles are evident for the first three panels, (A), (B), and (C). However after a pressure increase to 4×10^{-8} mbar, panel (D), the spectrum that results is identical to the previous 2×10^{-8} mbar spectrum, panel (C). We therefore take the panel (C) and (D) spectra to be that of the saturated adlayer and assign this ''relative'' coverage as $\Theta=1.0$. Further we shall assume that the integrated absorbance is directly proportional to coverage. (We will explore this assumption later.) This enables us to estimate the extent of coverage for each spectrum. Accordingly values of Θ, with relative precision of $\pm5\%$, are indicated on the panels.

In considering the first three panels, it is apparent that considerable spectroscopic changes occur within 10% of saturation coverage. In panel (A) in the ν_3 region, eight features (1322, 1325, 1328, 1330, 1333, 1335, 1343, and 1346 cm^{-1}) have bandwidths of $\Gamma\sim1$ cm^{-1} (full width at half band maximum). These sharp features are atop a diffuse, $\Gamma\sim30$ cm^{-1}, absorption centered near 1330 cm^{-1}. A compa-

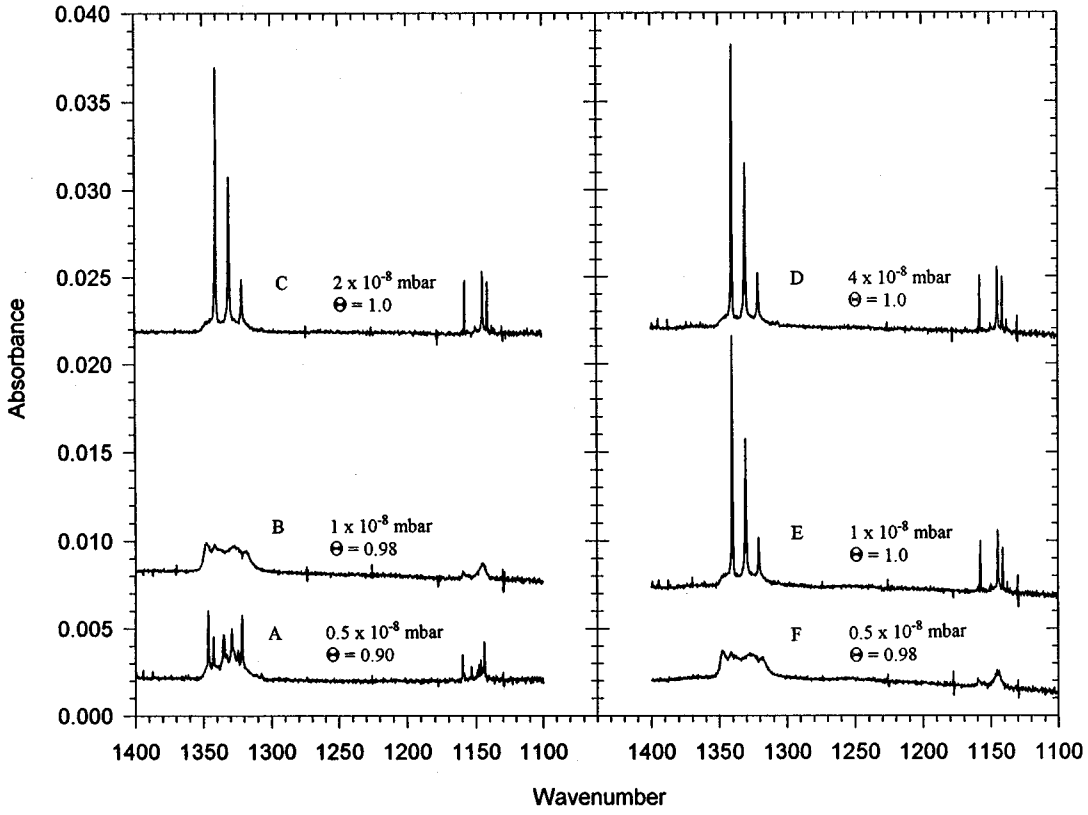

FIG. 1. Varieties of stable SO_2 adlayer on NaCl(100) spectrum near saturation. The temperature was 106.3 K and values of SO_2 pressure and coverage are listed for each panel. The resting time for each pressure setting was (A) 160 min; (B) 45 min; (C) 110 min; (D) 85 min; (E) 45 min; (F) 60 min.

rable number of somewhat sharper features, $\Gamma \leqslant 1\ \mathrm{cm}^{-1}$, with underlying diffuse absorption, is also found in the ν_1 region. For a coverage increase from $\Theta=0.90$, panel (A), to $\Theta=0.98$, panel (B), a dramatic change in profile occurs. In both spectral regions, the sharp features dissolve into structured diffuse profiles. In ν_1 there is a doublet and in ν_3 an overlapping quartet. The individual features in these regions have bandwidths of typically $\Gamma \sim 5\ \mathrm{cm}^{-1}$, or five times wider than those of the $\Theta=0.90$ coverage. Transformation to the saturated, $\Theta=1.0$, coverage spectrum of panel (C) is again dramatic. Some of the diffuse absorbance in panel (B) is transferred into a triplet of sharp features in the ν_3 region while some of the diffuse absorption remains. (We present frequencies, bandwidths and band areas of saturated adlayer spectra in Table I, based on experiments to be discussed below.) None of the eight sharp ν_3 features of panel (A) are represented in panel (C). A similar transformation occurs in the ν_1 region. Here, three new, sharp resonances (with perhaps two weaker features) are also observed, again with underlying diffuse absorption. As we have noted, an increase in pressure from 2×10^{-8} to 4×10^{-8} mbar [panel (D)] does not change the spectroscopic profile.

TABLE I. SO_2 vibrational spectra.

Gas phase[a]		Adsorbed phase[b]			
$\tilde{\nu}$ (cm^{-1})		$\tilde{\nu}$ (cm^{-1})	Γ (cm^{-1})	$\tilde{A}_s$ (cm^{-1})	$\tilde{A}_p$ (cm^{-1})
$\tilde{\nu}_1$	1151	1157.4	0.4	0.0017	0.0013
		1144.6	0.5	0.0039	0.0020
		1141.0	0.3	0.0037	0.0015
		1145	10	0.0060	0.0028
$\tilde{\nu}_3$	1362	1340.2	0.7	0.013	0.012
		1330.5	1.0	0.007	0.010
		1320.9	1.1	0.006	0.003
		1330	30	0.025	0.018

[a]T. Shimanouchi, *Tables of Molecular Vibrational Frequencies, Consolidated Volume 1* (National Standard Reference Data System, Washington, D.C., 1972).
[b]SO_2 on NaCl(100) at 110 K, see Fig. 3.

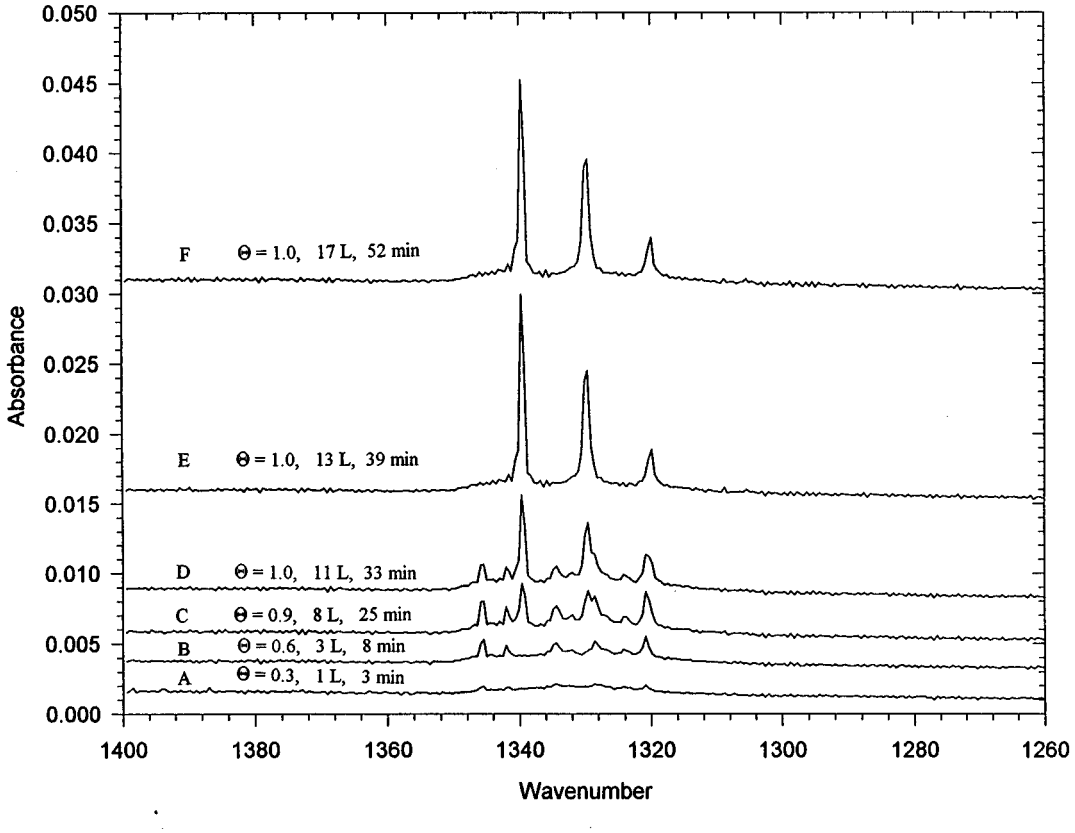

FIG. 2. Transient SO_2 adlayer on NaCl(100) spectra during slow dosing. The temperature was 100 K with SO_2 pressure fixed at $0.7\pm0.2\times10^{-8}$ mbar. Values of dosage, coverage and times are listed on each panel.

When the pressure is decreased from 4×10^{-8} mbar hysteresis is evident. Reduction of the pressure to 1×10^{-8} mbar, panel (E), does not recover the spectrum reached by raising pressure to the same value, panel (B). This hysteresis clearly indicates that nonequilibrium conditions persist for 45 min. Reducing the pressure to 0.5×10^{-8} mbar for 60 min, represented in panel (F), gives not the profile of panel (A), for the identical pressure, but rather the panel (B) profile. A spectrum taken 30 min later, i.e., 1 h at 0.5×10^{-8} mbar, still gives a profile identical to that of panel (F) [or (B)].

In the second experiment, a pressure was chosen ($0.7\pm0.2\times10^{-8}$ mbar) such that the growth of a saturated adlayer took much longer than the collection of a low-resolution spectrum. A suitable temperature was found to be 100 K. Beginning at zero coverage, a series of spectra at E_P polarization and 1 cm^{-1} resolution were recorded as the layer appeared and stabilized. These are presented in Fig. 2, in order of elapsed time. The extent of dosage in Langmuir ($1\ L=1\times10^{-6}$ Torr s) and the duration of dosage are indicated on each panel. Considerable variations in spectral profiles are evident in the lower four panels (1 to 11 L). However, for the upper two panels (13 and 17 L) the spectra are stable. Since these panels are indistinguishable from panels (C), (D), and (E) of Fig. 1, we take these spectra to represent the saturated adlayer and assign this coverage as $\Theta=1.0$. The lower coverage spectra are scaled accordingly.

As we shall see, the relative contributions of sharp and diffuse features are important to understanding the structure of the adlayer. In partitioning the total integrated absorbance into sharp features and diffuse absorption, our procedure was to fit a Lorentzian profile to each sharp feature, from which the bandcenter ($\tilde{\nu}$), bandwidth (Γ), and integrated absorbance ($\tilde{A}_s$ or $\tilde{A}_p$) could be evaluated. The diffuse band was fit to a Gaussian profile. Beginning with the final spectra at full coverage, the sharp features contribute $\Theta_s=0.50\pm0.05$ to the total coverage and the diffuse features also contribute $\Theta_d=0.50\pm0.05$. Thus the total integrated absorbance is equally partitioned between sharp and diffuse features. As we show in later experiments and in the listings of Table I, this even partitioning is roughly followed for E_s polarized measurements of ν_3 and both polarizations in the ν_1 region.

The diffuse feature grows in more rapidly at low coverage. For the $\Theta=0.3$ spectrum in Fig. 2, the diffuse band contributes $\Theta_d\approx0.25$ while the barely discernable sharp features, contribute only $\Theta_s\approx0.05$. As the coverage doubles to $\Theta=0.6$, the sharp contributions have tripled to $\Theta_s\approx0.15$ while the diffuse feature has doubled to $\Theta_d\approx0.45$. At this coverage the diffuse feature is, within experimental error, at its saturation value of $\Theta_d\approx0.5$. The octet of sharp features match, in frequency and relative absorbance, those of panel (A) in Fig. 1. For the coverage increase to $\Theta=0.9$, the triplet of sharp features that characterize the saturated adlayer have now appeared and overlap the original octet.

The changes between the 11 and 13 L spectra occur at

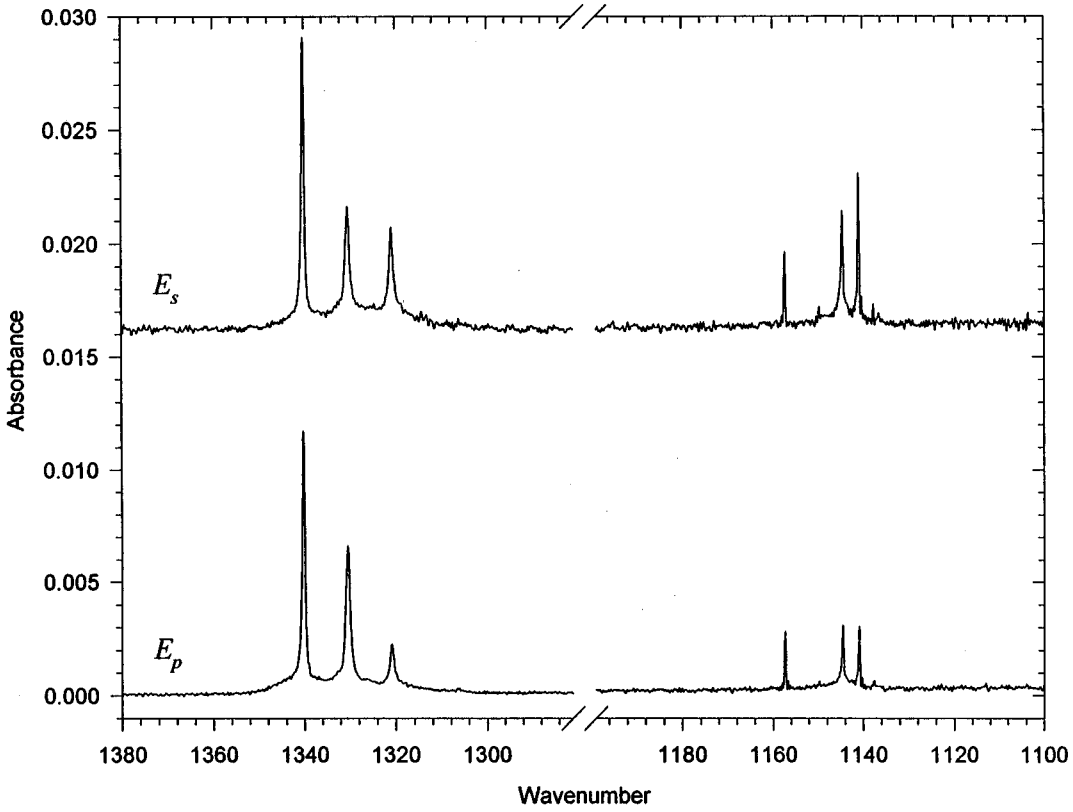

FIG. 3. Dependence of monolayer SO_2 on NaCl(100) spectra on polarization. The temperature was 110 K. See Table I for quantitative data.

saturated coverage, $\Theta=1.0$. The diffuse feature is invariant and its contribution to the total coverage, $\Theta_d=0.50$, is also invariant. While the total coverage contribution from the sharp features is also $\Theta_s=0.50$, the octet of resonances has transformed into a triplet with dosage and/or time. It is as if the molecules responsible for the sharp octet have undergone a rearrangement on the surface and/or an exchange with the gas phase molecules.

The third experimental was a comparison of E_s and E_p polarized spectra. The spectral resolution of 0.5 cm^{-1} was high enough to avoid any distortion in the ν_3 region; band shapes near ν_1 may be instrument limited. Here, the crystals were at 110 K, the SO_2 pressure was maintained at 3×10^{-7} mbar and the coverage was saturated. The spectra are presented in Fig. 3. The familiar triplet of sharp features with an underlying diffuse band appears in the ν_3 region. A sharp triplet and diffuse band is also found for the ν_1 region. These spectroscopic data are listed in Table I. Several additional sharp features, near the noise level, are also observed.

A final experimental was designed to identify characteristics of the saturated spectrum which may depend on temperature. The saturated adlayer was prepared at 100 K, at which temperature exchange with the gas occurs on a timescale of minutes (Fig. 2). The layer was trapped by rapidly cooling the crystals to 10 K while pumping residual SO_2 gas from the vacuum chamber. The triplet in ν_3 remains; while the bandwidths are narrower than those at 110 K (some more than others), the integrated absorbance is conserved. Neither the spectral profile nor the integrated absorbance of the diffuse features has changed. For the ν_1 region, several new weak features appeared.

Discussion

Formation of the adlayer

The spectral changes observed with coverage for the SO_2 adlayer shown in Figs. 1 and 2 are not found in any other systems studied on NaCl(100). Continuous monotonic changes in bandwidth and frequency of a single feature with coverage are observed with CO on NaCl(100).[21] We interpret submonolayers of CO as randomly occupied. The local density of adsorbates, and consequently their static and dynamic couplings, depend continuously on coverage.[21,22] Other systems, such as CO_2 or CH_4 on NaCl(100), form islands at submonolayer coverage. The density of adsorbates within an island, and thus the intermolecular coupling (excluding domain-edge effects), do not depend on coverage. The submonolayer spectra are sharp multiplets with the same splittings as the full-coverage case. Entirely diffuse and coverage-independent spectra have been observed for HBr[23] and H_2O[10] on salt surfaces; these adsorbates form amorphous hydrogen-bonded clusters. Thus the literature contains examples of two-dimensional gases, crystals, and glasses forming on NaCl(100). These phases yield qualitatively distinct spectra in the infrared. The presence of both diffuse and

sharp features whose relative absorbances and frequencies change with coverage is a puzzling phenomenon.

The spectrum of Fig. 1, panel (C), has been associated with a saturated adlayer, $\Theta=1.0$. As we shall later show by a photometric argument, this adlayer corresponds to about one SO_2 molecule per Na^+Cl^- ion pair on the (100) face. Additional evidence that it is not a multilayer is provided by a comparison with the infrared spectroscopy of films of SO_2, with their distinct set of frequencies and bandwidths.[14,15] Indeed, an extrapolation of the vapor pressure data[24] of solid SO_2 to 106.3 K suggests that the bulk solid should not form until a pressure of 10^{-7} mbar is reached. Moreover, that no additional features appear when the pressure is doubled [compare panels (C) and (D) of Fig. 1] suggests that additional SO_2 molecules are reluctant to adsorb to the saturated adlayer. We shall consider the saturated adlayer as monolayer SO_2 on NaCl(100).

The monolayer spectrum represents a uniquely stable condition of the adsorbate. It can be reached via various initial conditions of pressure, temperature, and coverage. Consider, however, the cases in Fig. 1 in which different spectra are observed under the same thermodynamic conditions. In these cases [panels (B) and (E), (A) and (F)] it is certain that the spectra cannot both represent equilibrated phases; perhaps neither one does. Our task in the following discussion is to reconcile the observed robustness of the monolayer with the evidence that it is kinetically trapped. To this end we consider the sharp and diffuse resonances to represent subpopulations of molecules (as opposed to being, say, part of one bizarre excitonic band shape). Then the sharp features represent molecules that equilibrate on a timescale short in comparison to the experiment (minutes), and their qualities are assured by phase equilibrium. The molecules responsible for the diffuse signal must equilibrate on a timescale longer then the experiment (hours).

The failure to achieve equilibrium conditions may be rationalized by estimations of the desorption rate τ^{-1}. We use the Arrhenius[25] relationship, $\tau^{-1}=\tau_0^{-1}\exp[-D_0/RT]$, where D_0 is the adsorbate binding energy and τ_0^{-1} the SO_2 vibrational frequency against the adsorbate bond. Taking $-D_0$ to be approximated by the isosteric heat of adsorption, $\Delta H=-32\pm4$ kJ/mol[17] and $\tau_0^{-1}=10^{13}$ s^{-1}, a typical absorbate frequency,[25] we find a range of adsorbate residence times from τ of 6 s to 14 h consistent with the experimental error limits on ΔH. Thus a tightly bound SO_2 adsorbate, e.g., $\Delta H=-36$ kJ mol^{-1}, would take an exceedingly long time to desorb. On the other hand, a more weakly bound adsorbate, e.g., $\Delta H=-28$ kJ mol^{-1}, can desorb in a few seconds.

The experiments represented in Fig. 2 contain information on the kinetics of adlayer formation. Consider the $\Theta=0.3$ coverage that accumulates in 3 min at 0.7×10^{-8} mbar and 100 K. We use the gas-kinetics expression, $Z_w=p/(2\pi mkT)^{1/2}$,[25] for the surface collision frequency (m^{-2} s^{-1}) where m is the molecular mass of SO_2. We find $Z_w=2\times10^{16}$ m^{-2} s^{-1} for the pressure/temperature of the second experimental set. For a period of 180 s (3 min) this corresponds to 4×10^{18} m^{-2} molecules striking the surface. At an available site density of $S=6\times10^{18}$ m^{-2} (the density of exposed Na^+Cl^- pairs[7]) this would correspond to a coverage of $\Theta=0.7$ for unit accommodation coefficient. The observed coverage of $\Theta=0.3$ implies a relatively high sticking efficiency of ~50%. Thus a reasonable scenario is that a good fraction of molecules stick when they strike the low coverage surface. And when they stick, although they may diffuse or reorientate on the surface, they remain stuck for hours. These molecules form an amorphous phase. The resulting spectrum is diffuse.

At higher coverages, say $\Theta=0.6$ to $\Theta=0.9$, the coverage has only increased by 50% yet the dosage has nearly tripled (3 to 8 L). Since the dosage greatly exceeds that needed for monolayer coverage, some molecules initially sticking must be desorbing on a time scale of minutes. Since the diffuse band has stopped growing we may imagine that an equilibrium now is being established for the more weakly bound molecules. Since there are two distinct sets of sharp features, the octet and the triplet, two phases may be represented. Since the characteristic triplet develops to saturation in ~6 min (compare the 11 and 13 L panels) this is the time scale for establishing equilibrium for the weakly bound molecules in this sublattice.

Spectroscopic profiles offer some clues as to the structure of the adlayer. Diffuse features are consistent with disordered structures. This has been predicted for spectra of fractals and randomly occupied sites by Wales and Ewing.[26] The interpretation of the initial sharp features is not obvious. The eight features for $\Theta=0.3$ and $\Theta=0.6$ coverages are identical in position and relative absorbance to those of panel (A) in Fig. 1. These features, growing in unison, have more than doubled with the doubling of coverage. That these features grow together suggest some possibilities. One is that there are eight distinct sites in the submonolayer. Alternatively islands are forming that can be described by eight molecules per unit mesh within the island. The islands, if they appear as long and narrow, might be described as stripes. Stripes in submonolayer systems have been discussed theoretically[27] and have been observed for films of large organic molecules in the laboratory.[28]

As the coverage is increased to $\Theta=0.9$ the octet of features has grown only slightly, but the triplet that signals the monolayer has begun to grow in. At $\Theta=1.0$, after 11 L and 33 min, the triplet dominates. After an additional 6 min, there has been no coverage increase, yet the octet of features has disappeared with its absorbance being transferred to the triplet. The underlying diffuse band has undergone no noticeable change. A possible rationale for the transformation of the structure giving rise to the spectroscopic octet to the structure that yield a triplet is crowding.

Photometry

Analysis of the polarized infrared spectra provide important clues to the structure of the saturated adlayer.

We can say at once that the calculations by Ron and Folman[17] for *single* SO_2 on NaCl(100) are inappropriate for the adlayer. Their results showed the adsorbed molecule as a dipod with its molecular axis is normal to the surface. This

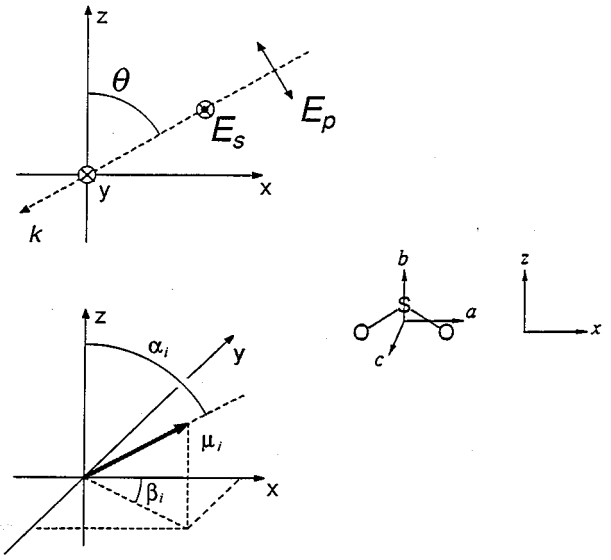

FIG. 4. The coordinate system.

means that the transition dipole associated with ν_1 (along the b axis or molecular z axis, see Fig. 4) must also be aligned with the surface normal. The corresponding resonance would appear in E_P spectra only, not in E_s.[1–5] As we see in Fig. 3, all features appearing in E_P polarization for the ν_1 region also have absorption in E_s polarization.

We can place the structure determination in quantitative form by considering the relationships between the polarized integrated absorbance and molecular cross sections. For the coordinate systems refer to Fig. 4, where the laboratory frame (locked to the crystal) are given by X,Y,Z and the molecular axes are x,y,z. As shown elsewhere[5,29,30] the relationship between the integrated absorption with E_p and E_s polarizations and the integrated cross sections are given by

$$\widetilde{A}_{P_i}=\frac{NS}{(2.303)\cos\,\theta}\left[\frac{\overline{\sigma_{Z_i}}\,\sin^2\,\theta}{(1+\overline{\alpha}U_{\perp}^0)^2}+\frac{\overline{\sigma_{X_i}}\,\cos^2\,\theta}{(1+\alpha U_{\parallel}^0)^2}\right], \quad (1)$$

$$\widetilde{A}_{S_i}=\frac{2NS\overline{\sigma_{Y_i}}}{(2.303)\cos\,\theta(1+\eta^2)(1+\overline{\alpha}U_{\parallel}^0)^2}. \quad (2)$$

Here, $N=4$ is the number of crystal faces interrogated and $\theta=60°$ is their tilt with respect to the interrogating radiation. The index of refraction of the NaCl substrate is $\eta=1.52$.[31] The site density of the adlayer is S. Expressions (1) and (2) differ somewhat from those originally given by Berg and Ewing,[30] who treated the molecules as an oriented gas. Dipoles induced perpendicular to the adlayer (in the Z direction) are accounted for by the term $(1+\overline{\alpha}U_{\perp}^0)^2$.[29,32] Here, $\overline{\alpha}$ is the mean polarizability of the adlayer and $U_{\perp}^0=S_3a^{-3}$ sums the induced dipoles in the adlayer. The lattice constant for a square is a, and $S_3=9.0336$ is the corresponding Ewald sum.[33] Dipoles induced in the plane of the adlayer (the X,Y plane) make use of the relationship $U_{\parallel}^0=-(\frac{1}{2})U_{\perp}^0$.[34] We distinguish the vibrational modes by i, where $i=1$ for the ν_1 mode and $i=3$ for the ν_3 mode.

The integrated cross sections refer to the laboratory or crystal fixed coordinates and are related to the molecular frame through

$$\begin{aligned}\overline{\sigma_{X_i}}&=3/2\overline{\sigma_{g_i}}\,\sin^2\,\alpha_i,\\ \overline{\sigma_{Y_i}}&=3/2\overline{\sigma_{g_i}}\,\sin^2\,\alpha_i,\\ \overline{\sigma_{Z_i}}&=3\overline{\sigma_{g_i}}\,\cos^2\,\alpha_i,\end{aligned} \quad (3)$$

where $\overline{\sigma_{g_i}}$ is the molecular integrated cross section for mode i. The direction of the transition dipole, μ_i, in the molecular frame (expressed through the integrated cross section) is carried to the laboratory frame through the direction sines and cosines in terms of angle α_i as shown in Fig. 4. Combination of Eqs. (1)–(3) allows for the determination of tilt angle α_i from

$$\alpha_i=\tan^{-1}\left\{\frac{[6(1+\overline{\alpha}U_{\parallel}^0)^2/(1+\overline{\alpha}U_{\perp}^0)^2]}{[8(\widetilde{A}_{P_i}/\widetilde{A}_{S_i})/(1+\eta^2)-1]^{1/2}}\right\}. \quad (4)$$

We can now use Eq. (4) to determine the tilt angles for adsorbed SO_2. We begin with the ν_1 mode. Here, the transition dipole is aligned along the symmetry axis (the z or b axis of Fig. 4). We take $\overline{\alpha}=3.94\times10^{-30}$ m^3 [31] with $U_{\perp}^0=0.14\times10^{30}$ m^3 and $U_{\parallel}^0=-0.07\times10^{30}$ m^3, having used the Ewald sum for the square lattice with constant $a=356$ pm, the distance between neighboring Na^+ ions in the (100) face.[7] Use of this value of a for the SO_2 adlayer assumes that the molecules are arranged on a square lattice with the same nearest neighbor separation as Na^+ (or Cl^-) ions in the surface below. For an average tilt angle, we use the sum of both sharp and diffuse features in Table I, $\widetilde{A}_P/\widetilde{A}_S=0.48\pm0.04$, to obtain $\alpha_1=73\pm6°$. Thus on an average, the b axis of the molecules is sharply tilted from the surface normal. The average tilt of the x or a axis is obtained from photometry of the ν_3 mode. Again using the sum of the integrated absorbances of sharp and diffuse features we find $\widetilde{A}_P/\widetilde{A}_S=0.84\pm0.08$ and obtain $\alpha_3=52°\pm3°$. Because shape and diffuse resonances contribute equally to each multiplet, considering them separately would yield approximately the same values of α_1 and α_3. This determination is consistent with monopodal structures. (If all molecules were dipods then $\alpha_3=90°$.) The analysis does not exclude mixtures of monopod and dipod adsorbates or other bonding arrangements.

Spectroscopy and possible SO_2 adlayer structures

It is difficult to extract the details of the saturated SO_2 adlayer structure from the spectroscopic data using only Eq. (4). The observed triplets could arise either from site or correlation field effects. In the former case, molecules would be adsorbed to three different sites, each with its characteristic ionic substrate generated electric field (and other differing environmental influences due to dispersion, overlap, etc.), giving rise to three distinct vibrational frequencies. Site split-

tings have been observed in the C_2H_2 on NaCl(100) adlayer spectroscopy.[8] Alternatively, each SO_2 molecule could have an identical site, but the extended layer could have multiple molecules per unit cell. Correlation or exciton splittings are observed in CO_2 on NaCl(100)[3,4] and in the low temperature phase of CO on NaCl(100).[1,2] *Both* site and crystal field effects could be operating in the case of SO_2 on NaCl(100) to account for the weakly bound sublattice.

Just what form of weakly bound sublattice best matches the observations depends on the splitting mechanism. We sketch the two possibilities:

Correlation splitting would occur in vibrations within islands containing many closely packed molecules in uniform environments. If there are three or more molecules per unit mesh within the islands, a triplet of features is possible. That the three features grow uniformly with coverage (see Fig. 2) is consistent with island growth. The presence of correlation splitting then requires a high degree of molecular order within the islands.

However, one observation is not consistent with the correlation splitting argument. Since the correlation effect is usually a consequence of coupled transition dipoles, the frequency splittings should depend on the oscillator strength of the vibrational transition. Yet the splittings in the ν_1 and ν_3 regions are comparable, while their oscillator strengths differ by a factor of 5.[35] It is possible that the different transition dipole orientations for the ν_1 and ν_3 modes could offset the differences in oscillator strengths. It is also possible that couplings occur through molecular properties other than transition dipoles.

Site splittings would require three different bonding arrangements for molecules to yield absorbance triplets in the sublattice. These sites can be randomly placed, but each of the three sites needs to have its own unique homogeneous environment as defined by nearest neighbor absorbates and the underlying NaCl(100) substrate. The three homogeneous environments are required to explain the small bandwidths of the triplets. The random placement of the different sites is then consistent with a disordered sublattice.

If the sharp absorbances are determined by their site environments and there is no transition dipole coupling among molecules in the adlayer, then each feature should have a weak satellite at a predictable frequency and absorbance due to vibration of the naturally occurring heavy isotope $^{34}SO_2$. The relative absorbance of each satellite, determined by the abundance of this isotope, should be 4%[36] of its parent. The ν_1 satellite features should be 7 cm^{-1} below the normal isotope vibrational frequency and 17 cm^{-1} downshifted from the ν_3 parent absorbances.[37]

A search for these satellites is rewarded in the E_p polarization of ν_3 of Fig. 3 with its favorable signal to noise ratio. A weak feature is found at 1307 cm^{-1} a possible partner to 1320.9 cm^{-1}, and the faint absorbance 1326 cm^{-1} a likely satellite of 1340.2 cm^{-1}. The frequency shift of 14 cm^{-1} is comparable to the predicted isotopic shift of 17 cm^{-1}. The partner for 1320.5 cm^{-1} expected in the region 1313 to 1316 cm^{-1} is not apparent in Fig. 3, however, its absorbance is predicted near the noise level. Possible candidates for satellites in the weak features of the ν_1 region can also be found. That those satellites assigned are at frequencies somewhat different from those predicted for the isolated isotopes can be rationalized by transition dipole coupling effects that are operating to a certain extent in the adlayer. Likewise absorbance anomalies, that can cause increases or decreases, are a consequence of coupling effects.[1–4] Thus while the weak features observed are consistent with heterogeneous site hypothesis they certainly do not prove it.

One observation speaks against site splittings. The three sites would be expected to have different bonding energies. Some sites would then be filled before others. Yet we always observe triplet absorption features to grow in unison (see Fig. 1).

The spectroscopic interpretations are then equivocal on the structure of the ordered array.

We can estimate the extent of surface coverage by using Eqs. (1)–(3). Because its absorbance is greater we shall consider the calculation from the ν_3 mode. From gas phase measurements[35] we use $\overline{\sigma_g}=3.1\times10^{-17}$ m molec^{-1} and taking $\alpha_3=52°\pm3°$ we find $\overline{\sigma_Z}=3.8\times10^{-17}$ m molec^{-1} and $\overline{\sigma_Y}=\overline{\sigma_X}=2.7\times10^{-17}$ m molec^{-1}. Using $\tilde{A}_P=0.043\pm0.005$ cm^{-1} (4.2 m^{-1}) from Table I (for both sharp and diffuse features) and Eq. (1) we find $S=5.0\pm0.5\times10^{18}$ molec m^{-2}. An analogous analysis from $\tilde{A}_P$ (both sharp and diffuse features) from the ν_1 region yields $S=7.2\pm0.7\times10^{18}$ molec m^{-2}. The site density of the (100) face (Na^+ or Cl^- ions) is 6.1×10^{18} molec m^{-2}. Within the expected perturbations of the intrinsic oscillator strength by the strong electric fields at the surface[29,38] the calculated values of S are consistent with each Na^+Cl^- pair covered by one SO_2 molecule. Estimates of S from the $\tilde{A}_S$ values are also consistent with this conclusion.

We turn now to a theoretical investigation of the SO_2 adlayer.

THEORETICAL ANALYSES

Our strategy in this section is first to describe the calculation of potential functions between SO_2 molecular dimers and SO_2 molecules with the NaCl substrate. These potential functions are then used to calculate the binding of a single SO_2 molecule with the surface and the binding of clusters of SO_2 molecules with the surface. Next a Monte Carlo calculation is described to explore theoretical equilibrium adlayer structures for $\Theta=0.5$ and $\Theta=1.0$ coverages.

The potential surface of the SO_2 dimer has been studied in some detail,[18] and the key feature that emerges is that the surface is very flat, without well defined minima. Indeed, the most accurate calculations were unable to determine conclusively which of the low energy stationary points is the global minimum, since calculation at different levels of theory and with different basis sets reach different conclusions. Consequently, we may expect that the interactions between the molecules will not lead to well-ordered structures, even though they may contribute significantly to the binding energy.

TABLE II. Positions of sites within SO_2 molecule, expressed in pm relative to center of mass.

Site	x	y	z
SO_2	0.0000	0.0000	0.0000
S	0.0000	0.0000	0.3605
O	±123.74	0.0000	−36.05
S′	0.0000	0.0000	51.65
O′	±113.56	0.0000	−30.96

TABLE IV. Comparison between the rotational constants and binding energy of the SO_2 dimer, calculated using this potential, with those measured experimentally or calculated by *ab initio* methods.

	Experiment[a]	*Ab initio*[b] (MP2-TZ2P)	This work
A (MHz)	6958.5		7143
B (MHz)	948.5		846
C (MHz)	903.8		810
D_e (kJ mol^{-1})		−9.1	−9.3

[a]Reference 19.
[b]Reference 18.

Potential functions

We have constructed a model of the potential function for $SO_2\cdots SO_2$ and $SO_2\cdots$surface interactions. The charge distribution of the SO_2 molecule is described by a five-center distributed multipole analysis (DMA) with multipole sites at the nuclei and the bond centers. Multipoles to rank 4 (hexadecapole) were calculated for each site at MP2 using the basis of McLean and Chandler[39] ($6s5p2d$ on S and $4s2p1d$ on O). This basis gave an overlap dipole of 1.350 D (4.503×10^{-30} C m) and quadrupoles Θ_{xx}, Θ_{yy}, and Θ_{zz} of −15.18, 12.64, and 2.54, respectively (in units of 10^{-40} C m^2); these compare reasonably well with the experimental value of the dipole[40] of 1.633 D (5.447×10^{-30} C m), and the quadrupoles[41] of −16.38, 12.88, and 3.40 (again in units of 10^{-40} C m^2.) The polarizability of the SO_2 molecule was described by the three-site distribution polarizabilities calculated by Le Sueur.[42] The repulsive potential between the SO_2 molecules uses an atom–atom description of the form

$$U_{\text{rep}}=\sum_{ab} K\,\exp(-\alpha_{ab}(R_{ab}-\rho_{ab})), \tag{5}$$

where $K=10^{-3}$ hartree and the parameters α_{ab} and ρ_{ab}, which may depend on the relative orientations of sites a and b, were determined by the test-particle method of Stone and Tong.[36] In our model α_{ab} and ρ_{ab} are taken to be independent of orientation, but the sites were moved away from the nuclei to describe the distortion of the atoms resulting from bond formation. The positions of the sites, relative to the center of mass, are presented in Table II. The test-particle values for the ρ_{ab} and α_{ab} parameters were checked by performing a small number of calculations on the SO_2 dimer using the IMPT method of Hayes and Stone[44] to determine the repulsion energy. In the light of these calculations the ρ_{ab} were adjusted slightly. The final values of the parameters are given in Table III.

A reliable treatment of the dispersion is important but difficult to achieve. We have calculated isotropic C_6 and C_8 coefficients for the molecule using coupled Hartree–Fock perturbation theory as implemented in CADPAC.[45] We used a near Hartree–Fock basis set due to Maroulis,[46] $13s9p2d$ contracted to $11s7p2d$ on S, and $8s6p2d$ contracted to $6s4p2d$ on O. This gives a mean dipole polarizability of 23.62 a.u., which is 7% smaller than the experimental value[47] of 25.60, and a C_6 coefficient of 265.1 a.u. compared with the value of 294 a.u. determined by Kumar and Meath[48] from dipole oscillator strength distributions. The C_8 coefficient is calculated to be 14515 a.u. with the origin at the center of mass. For C_{10} we used the relation[49]

$$C_{10}\simeq\frac{1.225C_8^2}{C_6}, \tag{6}$$

where we have used the experimental value for C_6.

The anisotropy of the dispersion interaction is likely to be quite important for SO_2, especially as the other contributions to the potential are not very anisotropic. We have attempted to represent the anisotropy by using a site–site expression for the dispersion

$$U_{\text{disp}}=\sum_{ab} f_6^{ab}\frac{C_6^{ab}}{R^6}+f_8^{ab}\frac{C_8^{ab}}{R^8}+f_{10}^{ab}\frac{C_{10}^{ab}}{R^{10}}, \tag{7}$$

where $CS_6^{S\cdots S}+4C_6^{S\cdots O}+4C_6^{O\cdots O}$ reproduces the molecular C_6, and similarly for C_8 and C_{10}. The partitioning into site–site terms was guided by the ratio of the distributed polarizabilities. The resulting values are listed in Table III. The f_n in the above equation are Tang–Toennies damping functions

$$f_n^{ab}(R)=P(n+1,s\alpha_{ab}R), \tag{8}$$

where α_{ab} is the hardness parameter in the repulsive term and $s=0.575$ is a scale factor, chosen to reproduce the experimental rotational constants[19] and the calculated binding energy[20] of the dimer. These quantities are listed in Table IV.

TABLE III. $SO_2\cdots SO_2$ repulsion and dispersion interaction parameters.

$SO_2\cdots SO_2$						
i	j	C_6^{ij} (kJ mol^{-1}) pm^6	C_8^{ij} (kJ mol^{-1}) pm^8	C_{10}^{ij} (kJ mol^{-1}) pm^{10}	α_{ij} (nm^{-1})	ρ_{ij} (pm^{-1})
S′	S′	-1.8457×10^{15}	-3.4912×10^{20}	$-768\,197\times10^{20}$	35.07	36.13
S′	O′	-1.8736×10^{15}	-2.7767×10^{20}	$-488\,852\times10^{20}$	38.70	33.67
O′	O′	-1.9020×10^{15}	-2.2084×10^{20}	$-311\,088\times10^{20}$	43.16	31.69

TABLE V. $SO_2\cdots NaCl$ repulsion-penetration and dispersion interaction parameters.

$SO_2\cdots NaCl$				
i	j	C_6^{ij} (kJ mol^{-1}) pm^6	α_{ij} (nm^{-1})	ρ_{ij} (pm^{-1})
SO_2	Na^+	-1.216×10^{15}		
SO_2	Cl^-	-1.2483×10^{15}		
S	Na^+		53.29	312.0
S	Cl^-		44.44	376.7
O	Na^+		47.21	266.8
O	Cl^-		33.77	357.3

The repulsion potential for the interaction of the SO_2 molecules with the surface ions was calculated by the IMPT method.[44] For the $SO_2\cdots Na^+$ repulsion, a $2s1p$ Na^+ basis was used, comprising the occupied orbitals obtained for the free Na^+ ion using the $10s6p$ basis of Huzinaga.[50] The repulsion energy involves only the occupied orbitals; justification for the taking a free Na^+ ion as typical of an ion in a lattice comes from the practically identical dipole polarizabilities of the free Na^+ and the Na^+ ion in NaCl.[47]

The Cl^- ion in the lattice is very different from the free Cl^-.[51] The Cl^- basis was abstracted from a calculation on a cluster. A Cl^- ion, surrounded by 6 Na^+ ions, was embedded in a $5\times5\times5$ lattice of unit charges. We used the contracted basis on the Na^+ ions as derived for the free ion, and a 8-6311 G basis for Cl^-, optimized for the bulk by Saunders.[52] From the eigenfunctions of the cluster we identified those orbitals which primarily belonged to the Cl^- ion, abstracting orbitals that could be identified as the $1s$, $2s$, $2p$, $3s$, and $3p$ orbitals to give us the $3s2p$ basis.

This procedure leads to occupied orbitals suitable for the bulk NaCl crystal. Calculations by Hutson and Fowler[53] show however that the anion size and average polarizability at the surface are very similar to those in the bulk.

The $SO_2\cdots Na^+$ repulsion was calculated at 49 points and the $SO_2\cdots Cl^-$ repulsion at 21 points, and after addition of the correction for penetration, each was fitted to a site-site potential of the form given in Eq. (4). The parameters obtained are shown in Table V.

In the present study we calculated the electrostatic distribution of the NaCl(100) surface using the *ab initio* package CRYSTAL,[54] performing an all electron SCF calculation on a four layer slab. The Gaussian basis was based on the 8-6311 G basis of Saunders,[52] which had been reoptimized for the surface calculation, optimization being carried out with respect to the energy of a two layer slab. Multipoles were then assigned to the ions in the four layer slab using the partitioning scheme of Mulliken. The charge distribution was represented by multipoles up to quadrupole on each ion site. These multipoles were dominated by the charges, which were close to ±1, with the higher multipoles being relatively small.

Using a single center on the SO_2, located at the center of mass, the sites on the ionic centers, the dispersion coefficients for these site-site interactions were estimated using a geometric-mean combination rule. Data for the interactions came from the experimentally determined isotropic C_6 coefficient for the $SO_2\cdots SO_2$ interaction,[48] and the *ab initio* in-crystal dispersion coefficients calculated by Fowler and Pyper.[55] These parameters are reproduced in Table V. This contribution to the energy was undamped.

We did not include the higher order dispersion coefficients in this treatment. It seems likely that the topology of the surface–molecule interaction will be principally determined by the electrostatic and short-range terms. In the present study we are primarily interested in the structure, which will be more forgiving of these omissions. The omission of damping from the C_6 term will also compensate somewhat for the omission of the higher terms.

The surface was treated as of infinite extent in the (X,Y) plane, and comprised 20 layers in the Z direction. We used the experimentally determined crystal geometry. The longer ranged interactions between the molecules and the surface were summed using Fourier-series methods.[56–58]

Results and discussion

Single SO_2 on NaCl(100)

We minimized the energy of a single SO_2 molecule on the NaCl(100) substrate, ignoring the contribution to the total energy from induction. The induction energy, although quite important for the description of an isolated molecule on the surface, is expected to play a much less significant role for the interactions of a monolayer with a surface. This was shown by *ab initio* calculations on the $CO\cdots NaCl(100)$ system[59] where the induced moments, both for the surface and monolayer, were found to be very small for the $p(1\times1)$ structure. We attribute this to the unfavorable interactions between the induced moments on neighboring adsorbed molecules, which damps the response of the monolayer to the surface fields.

We found only one distinct minimum on the surface. The SO_2 molecule binds as a dipod with its symmetry axis normal to the surface, and its center of mass 303 pm above the surface plane. The molecule, with oxygen atoms down, bridges two Na^+ ions symmetrically and has a binding energy of -21.6 kJ mol^{-1}. While our dipod structure agrees with the earlier calculation of Ron and Folman,[17] their binding energy of -28.2 kJ mol^{-1} is somewhat larger.

If the SO_2 molecule is moved from one binding site to a neighboring one, optimizing orientation and height above the surface at each point on the path, the barrier is about 7 kJ mol^{-1}. Using the Arrhenius expression, with $\tau_0=10^{13}$ s^{-1} as before and the barrier for D_0, the time, τ, for site jumping at 100 K is only 40 ns so surface diffusion for single SO_2 molecules is rapid on the time scale of the experiments.

Adlayer SO_2 on NaCl(100)

One possible structure for the SO_2 layer that could account for the diffuse part of the spectrum might comprise SO_2 molecules each adsorbed in dipod fashion to two Na^+ ions, but arranged randomly over the surface. We con-

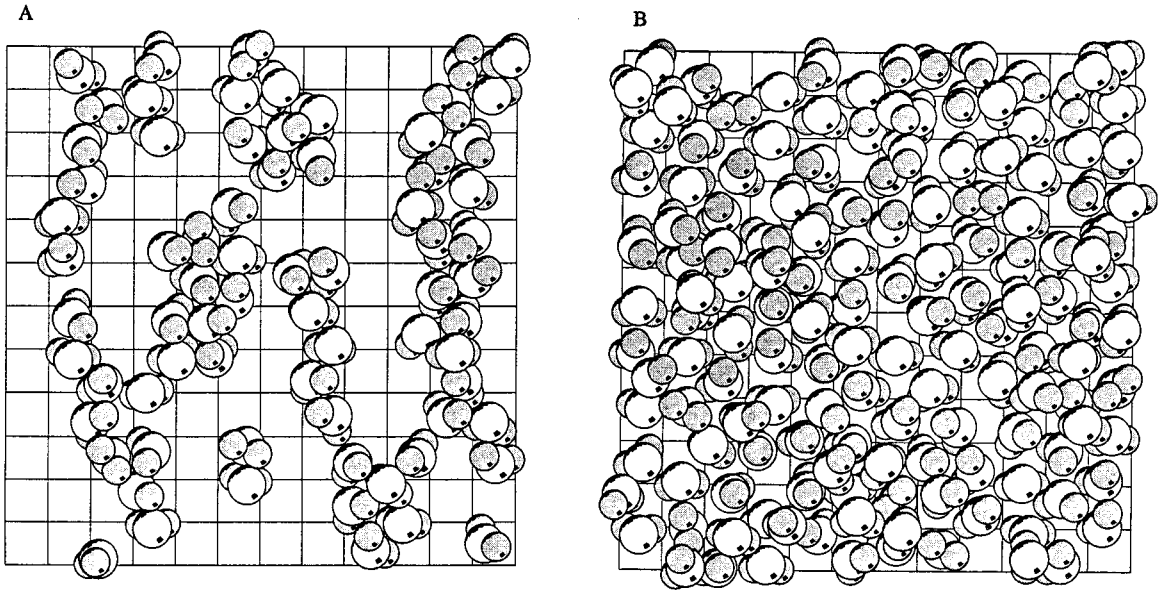

FIG. 5. The Monte Carlo calculations for $\Theta=0.5$ (panel A) and $\Theta=1.0$ (pand B). These figures were generated using the Molscript program [P. J. Kraulis, J. Appl. Cryst. **24**, 946 (1991)].

structed such an array by selecting pairs of adjacent sites at random on a 100×100 patch of NaCl. This led to a coverage of $\Theta=0.45$ (rather an $\Theta=0.50$ because isolated Na^+ sites remain) and it would be necessary to absorb a further half monolayer to reach the observed coverage. A random array of this sort has numerous sites at which molecules in the second layer might be adsorbed; we found 16 distinct types of site on the 100×100 patch. Adsorption energies at these sites, estimated by minimizing the energy of an additional molecule, varied from 10 to 30 kJ mol^{-1}. According to the Arrhenius desorption rate expression, these energies correspond to lifetimes ranging from milliseconds to minutes. One might suppose that the longer-lived molecules in the second layer were responsible for the sharp lines in the spectrum.

However, this is a grossly oversimplified picture. The photometry for the ν_1 mode shows that the molecules do not have their symmetry axes perpendicular to the surface, and it is hard to see how the supposed second layer could give rise to a sharp spectrum.

Monte Carlo calculations

In order to achieve a more realistic description, we carried out Monte Carlo calculations, in the canonical ensemble at 100 K, on a 12×12 patch of the surface, periodically replicated, using SO_2 coverages varying from $\Theta=0.50$ to 1.0. Each Monte Carlo step involved a change of a rotational or translational coordinate of one randomly chosen molecule, accepted or rejected using the standard Metropolis algorithm. N such steps, in a system with N SO_2 molecules, constituted one Monte Carlo cycle. The energy per molecule typically reached a stable value of about -2450 K(-20.4 kJ mol^{-1}) after 1000–2000 cycles, but we do not believe that full equilibration was achieved in any of the runs. (Note that the real system has not reached equilibrium at 100 K after 30 min.) Nevertheless, the results are instructive.

In one calculation the system was started at a coverage $\Theta=0.50$ in a regular array in which all the SO_2 molecules were aligned parallel to the crystal X axis as dipods, forming stripes in the Y direction. This configuration has an energy of -2200 K(-18.3 kJ mol^{-1}), somewhat higher than the equilibrium configurations, which are of the kind shown in Fig. 5(A). Here, the grid intersections indicate Na^+ sites and conventional van der Waals radii[60] have been chosen for O and S atoms. Although vestiges of the original strips remain, there is evidently a tendency for the molecules to diffuse across the surface and to aggregate into islands, and it is also notable that many of the molecules are no longer in the energetically favored dipod structure.

What is more striking is that a very similar outcome was observed when the system was started in a low-energy configuration in which the SO_2 molecules were arranged in a herringbone pattern reminiscent of the structure of a layer of molecules in the solid. In this case the energy, initially -2750 K(-22.9 kJ mol^{-1}) rose to -2450 (-20.4 kJ mol^{-1}) over the first 1000 or so cycles and stabilized at around the latter value. Clearly, therefore, the stabilization energy of the regular structure is not enough to overcome the entropic effects leading to disorder. In spite of the limitations of the Monte Carlo calculations, we believe that this provides strong evidence that the structure is disordered.

Progressive addition of further molecules, followed by equilibration, up to monolayer coverage led to configurations like that shown in Fig. 5(B). We see that although there are some molecules in dipod geometries, the general structure is highly disordered. The SO_2 molecules are not closely registered with the underlying Na^+ sites, showing that the inter-

actions between the SO_2 molecules play a strong role in determining the adlayer structure. At this coverage there is no movement of molecules from site to site (probably because the nature of the Monte Carlo step does not permit it) but there is substantial reorientation of many of the molecules in each cycle. It is not possible to identify the two classes of molecules that might be responsible, respectively, for the broad and sharp parts of the spectrum, nor is it possible to see how a mechanism such as exciton coupling in such a structure could lead to reproducible sharp lines as observed.

SYNTHESIS

Under the range of conditions studied here, the SO_2 adlayers were not fully equilibrated. This follows from the observed hysteresis in vibrational spectra as a function of pressure. When these conditions were simulated by Monte Carlo methods, a memory of the initial molecular configuration (long-range temporal order) persisted, without any tendency toward a crystalline state (long-range spatial order). In short, both the spectroscopic experiments and computational model satisfied some sufficient condition of nonequilibrium. Therefore we expect that the layers' microscopic properties depend on their histories of preparation.

The above conclusion is strictly true when accounting for all external degrees of freedom of the adsorbed molecules. Yet there is evidence from the Monte Carlo model that only a subset of these modes are kinetically trapped. At unit coverage individual adsorbates remain fixed in their sites (easily classified as monopods or dipods); most sodium ions are associated with a specific oxygen atom of SO_2. Within this constraint, however, many molecules rotate and reorient freely. The computational model also identifies the energetic basis of this behavior: There is a large difference between the overall depth of the adsorption potential and the contribution from orientational effects, with relevant thermal energies in between.

The observed vibrational spectra invite a parallel analysis. The optical cross-section of vibrational excitons in the monolayer is divided into a diffuse component that is independent of experimental conditions, and a component that responds to changing conditions with an interplay of sharp and diffuse resonances. In analogy to the computational results, we suggest that the diffuse spectral features reflect disorder frozen in during initial site selection. The sharp resonances, then, arise when the remaining (orientational) degrees of freedom establish limited long-range order. As this transition can be driven purely by pressure, it would seem to reflect those details of the adsorption potential that determine packing density in two dimensions. No such spatially ordered state appeared in the computational model. We note that the simulation included no analog to an enforced vapor pressure, and that the computation of SO_2 cluster geometries is notoriously difficult. A full account of the observed transition will require investigation by other means.

ACKNOWLEDGMENTS

This project was made possible with the help of others. Evamaria Cavaid performed the difficult experiments leading to Fig. 1. Kent Davis prepared Figs. 1–3. G.E.E. acknowledges financial support under NSF Grants No. CHE91-15444 and NSF CHE95-05892. G.E.E., A.J.S., and A.W.M. were able to travel and work together in Cambridge and Bloomington through a NATO Collaborative Research Grant No. 921151.

[1] D. Dai and G. E. Ewing, J. Electron Spectrosc. Relat. Phenom. **64/65**, 101 (1993), and previous work cited.
[2] J. Heidberg, M. Suhren, and H. Weiss, J. Electron Spectrosc. Relat. Phenom. **64/65**, 227 (1993), and previous work cited.
[3] O. Berg, G. E. Ewing, and R. Disselkamp, Surf. Sci. **227**, 8 (1992), and previous work cited.
[4] J. Heidberg, E. Kampshoff, R. Kühnemuth, and O. Schönekas, J. Electron Spectrosc. Relat. Phenom. **64/65**, 803 (1993), and previous work cited.
[5] L. Quattrocci and G. E. Ewing, J. Chem. Phys. **96**, 4205 (1992).
[6] S. K. Dunn and G. E. Ewing, J. Phys. Chem. **96**, 5284 (1992).
[7] H. K. Koski and E. Sandor, Acta Crystallogr. B **31**, 350 (1975).
[8] J. Heidberg and W. Häser, J. Electron Spectrosc. Relat. Phenom. **54/55**, 971 (1990).
[9] J. O. Hirschfelder, C. F. Curtiss, and R. B. Bird, *Molecular Theory of Gases and Liquids* (Wiley, New York, 1964).
[10] H. H. Landolt and R. Börnstein *Atom-und Molekularphysik 4. Teil, Kristable* (Springer, Berlin, 1955).
[11] B. Post, R. S. Schwartz, and I. Fankuck, Acta Cryst. **5**, 372 (1952).
[12] W. F. Giauque and C. C. Stephenson, J. Am. Chem. Soc. **60**, 1389 (1938).
[13] W. F. Giauque and W. M. Jones, J. Am. Chem. Soc. **70**, 120 (1948).
[14] F. Fleyfel, H. H. Richardson, and J. P. Devlin, J. Phys. Chem. **94**, 7032 (1990).
[15] R. K. Khanna, G. Zhao, M. J. Ospina, and J. C. Pearl, Spectrochim. Acta A **44**, 581 (1988).
[16] A. Anderson and M. C. W. Campbell, J. Chem. Phys. **67**, 4300 (1977).
[17] T. Ron and M. Folman, J. Phys. Chem. **75**, 2602 (1971).
[18] R. G. A. Bone, C. R. Le Sueur, R. D. Amos, and A. J. Stone, J. Chem. Phys. **96**, 8390 (1992).
[19] A. Taleb-Bendiab, K. W. Hillig II, and R. L. Kuckowski, J. Chem. Phys. **94**, 6956 (1991).
[20] *Product and Vacuum Technology Reference Book* (Leybold Inc., San Jose, 1990).
[21] C. Noda and G. E. Ewing, Surf. Sci. **240**, 181 (1990).
[22] R. Disselkamp, H.-C. Chang, and G. E. Ewing, Surf. Sci. **240**, 193 (1960).
[23] P. M. Blass, R. C. Jackson, J. C. Polanyi, and H. Weiss, J. Chem. Phys. **94**, 7003 (1991).
[24] R. E. Honig and H. O. Hook, RCA Rev. **21**, 360 (1960).
[25] P. W. Atkins, *Physical Chemistry*, 4th ed. (Freeman, New York, 1990).
[26] D. J. Wales and G. E. Ewing, J. Chem. Soc. Faraday Trans. **88**, 1359 (1992).
[27] M. M. Hurley and S. J. Singer, J. Phys. Chem. **96**, 1938 (1992), 1951.
[28] C. M. Knobler and R. C. Desai, Annu. Rev. Phys. Chem. **43**, 207 (1992).
[29] H. H. Richardson, H.-C. Chang, C. Noda, and G. E. Ewing, Surf. Sci. **216**, 93 (1989).
[30] O. Berg and G. E. Ewing, Surf. Sci. **220**, 207 (1989).
[31] E. D. Palik, *Handbook of Optical Constants of Solids* (Academic, New York, 1985).
[32] W. Chen and W. L. Schaich, Surf. Sci. **218**, 580 (1989).
[33] B. M. E. van der Hoff and G. C. Benson, Can. J. Phys. **31**, 1087 (1953).
[34] W. M. Murphy, J. Raman Spectrosc. **11**, 339 (1981).
[35] C. Secroun, A. Barbe, and P. Joave, J. Mol. Spectrosc. **45**, 1 (1973).
[36] R. C. Weast, Ed., *Handbook of Chemistry and Physics* (Chemical Rubber, Cleveland, 1972).
[37] M. Allavena, R. Rysnik, D. White, V. Calder, and D. E. Mann, J. Chem. Phys. **50**, 3399 (1969).
[38] D. K. Lambert, J. Chem. Phys. **94**, 6237 (1991).
[39] A. D. McLean and G. S. Chandler, J. Chem. Phys. **72**, 5639 (1980).
[40] D. Patel, D. Margolese, and T. R. Dyke, J. Chem. Phys. **70**, 2740 (1979).
[41] A. W. Ellenbroek and A. Dymanus, Chem. Phys. Lett. **42**, 303 (1976).
[42] C. R. Le Sueur, Ph.D. thesis, University of Cambridge, England.

[43] A. J. Stone and C. S. Tong, J. Computational Chem. **15**, 1377 (1994).
[44] I. C. Hayes and A. J. Stone, Mol. Phys. **43**, 83 (1984).
[45] R. D. Amos and J. E. Rice, The Cambridge Analytical Derivatives Package issue 4.0.
[46] G. Maroulis, Chem. Phys. Lett. **198**, 112 (1992).
[47] A. Kumar and W. J. Meath, Can. J. Phys. **63**, 417 (1985).
[48] A. Kumar and W. J. Meath, Chem. Phys. **91**, 411 (1984).
[49] A. J. Thakkar, J. Chem. Phys. **89**, 2092 (1988).
[50] S. Huzinaga, J. Chem. Phys. **42**, 1293 (1965).
[51] P. W. Fowler and P. A. Madden, Phys. Rev. B **29**, 1035 (1984).
[52] V. R. Saunders (private communication).
[53] J. M. Hutson and P. W. Fowler, Surf. Sci. **173**, 337 (1986).
[54] C. Pisani, R. Dovesi, C. Roetti, M. Causa, and V. R. Saunders, Crystal 92.
[55] P. W. Fowler and N. C. Pyper, Mol. Phys. **49**, 317 (1986).
[56] P. H. Lambin and P. Senet, Int. J. Quantum Chem. **46**, 101 (1993).
[57] W. A. Steele, Surf. Sci. **36**, 317 (1973).
[58] T. H. M. van den Berg and A. van der Avoird, Chem. Phys. Lett. **160**, 223 (1989).
[59] A. W. Meredith, J. Chem. Phys. **104**, 3058 (1996).
[60] L. Pauling, *The Nature of the Chemical Bond* (Cornell University, Ithaca, 1960).